On Traveling Path and Related Problems for a Mobile Station in a Rechargeable Sensor Network

Liguang Xie
Department of Electrical and
Computer Engineering
Virginia Tech
Blacksburg, Virginia, USA
xie@vt.edu

Yi Shi
Intelligent Automation Inc. &
Virginia Tech
Rockville, Maryland, USA
yshi@vt.edu

Y. Thomas Hou [*]
Department of Electrical and
Computer Engineering
Virginia Tech
Blacksburg, Virginia, USA
thou@vt.edu

Wenjing Lou
Department of Computer
Science
Virginia Tech
Falls Church, Virginia, USA
wjlou@vt.edu

Hanif D. Sherali
Department of Industrial and
Systems Engineering
Virginia Tech
Blacksburg, Virginia, USA
hanifs@vt.edu

ABSTRACT

Wireless power transfer is a promising technology to fundamentally address energy problems in a wireless sensor network. To make such a technology work effectively, a vehicle is needed to carry a charger to travel inside the network. On the other hand, it has been well recognized that a mobile base station offers significant advantages over a fixed one. In this paper, we investigate an interesting problem of co-locating the mobile base station on the wireless charging vehicle. We study an optimization problem that jointly optimizes traveling path, stopping points, charging schedule, and flow routing. Our study is carried out in two steps. First, we study an idealized problem that assumes zero traveling time, and develop a provably near-optimal solution to this idealized problem. In the second step, we show how to develop a practical solution with non-zero traveling time and quantify the performance gap between this solution and the unknown optimal solution to the original problem.

Categories and Subject Descriptors

C.2.1 [**Computer-Communication Networks**]: Network Architecture and Design—*Wireless communication*; G.1.6 [**Numerical Analysis**]: Optimization—*Nonlinear programming, Linear programming*

Keywords

Modeling and optimization; nonlinear programming; wireless power transfer; mobile base station; wireless sensor network

---

[*]Please direct all correspondence to Prof. Tom Hou.

1. INTRODUCTION

Recently, wireless power transfer (WPT) has been demonstrated to be a promising technology to address energy problems in a wireless sensor network (WSN) [8, 10]. This new WPT technology was based on the so-called *magnetic resonant coupling* [3, 4], which allows electric energy to be transferred from a source to a number of receivers via a nonradiative magnetic resonant induction. The most attractive features of this WPT technology are high energy transfer efficiency even under omni-direction, not requiring line-of-sight, and being insensitive to the neighboring environment.

In [8, 10], the authors showed how a wireless charging vehicle (WCV) can support WPT by bringing an energy source charger to the proximity of sensor nodes and charging their batteries wirelessly. In those studies, the authors assumed a simple setting where the location of the base station is fixed. On the other hand, it has been well recognized in the sensor network community that a mobile base station (MBS) offers significant advantages over a static one (see, e.g., [1, 5, 7, 13]). Since a base station is the sink node for all data that are collected from the sensor nodes, a mobile base station helps alleviate the traffic relay burden from a fixed set of sensor nodes near the base station to other sensor nodes in the network, thus avoiding energy hot spots and prolonging network lifetime.

Allowing the base station to be mobile adds considerable complexity to the underlying problem. In the most general case, the MBS could travel separately from the WCV, which calls for a separate vehicle to carry the base station. Given that the energy consumption for a vehicle is likely to be the dominant component in the big picture of energy consumption, we do not advocate this approach and defer it to a future study. Instead, in this paper, we consider the case where the MBS is co-located with the WCV. This allows us to explore traveling related questions for only one vehicle while still enjoying the benefits associated with a MBS.

Specifically, we consider the following problem in this paper. Suppose the base station is co-located with the WCV and we call the combines objects simply as WCV when there is no ambiguity. There is a home service station for the WCV (see Fig. 1). The WCV follows a periodic schedule to travel inside the network for charging the sensor nodes. While traveling inside the network, the WCV makes a number of stops and charge sensor nodes near those stops. At any time, data collected from the sensor nodes are relayed
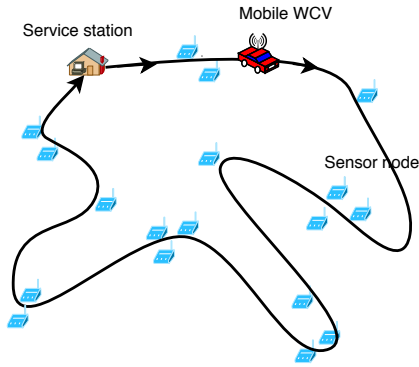
Figure 1: An example sensor network with a mobile WCV.

to the WCV (via multi-hop). By satisfying certain constraints, we hope that none of the sensor nodes in the network will ever run out of energy, i.e., the WSN will remain operational indefinitely.

Apparently, the above problem brings in a number of technical challenges. First of all, the traveling path for the WCV is unknown and needs to be determined. Second, we need to find the optimal stopping points along this path as well as the charging schedule of the WCV (i.e., how long it shall stay at each stopping point). Finally, the data flow routing in the network is dynamic and depends on where the WCV is in the network. Among these challenges, we find that the traveling path problem is most crucial and solutions to the other sub-problems all hinge upon the determination of a traveling path. In this paper, we address these challenges by studying an optimization problem.[1]

The main contributions of this paper are as follows:

- We formulate an optimization problem (TPP) that involves joint optimization of traveling path, stopping points, charging schedule, and data flow routing. This is shown to be a nonlinear program (NLP).

- To tackle TPP, we first consider an idealized problem (OPT-ub) that assumes zero traveling time (i.e., infinite traveling speed) from one point to another. The optimal solution of OPT-ub gives an upper bound to TPP.

- Subsequently, we develop a provably near-optimal solution to OPT-ub for any desired level of accuracy ϵ. Our solution involves several novel techniques, such as discretization of energy reception rate and energy consumption rate, double partitioning of the smallest enclosing disk (SED) into smaller subareas with tight upper energy consumption bounds and lower energy reception bounds, and representation of each subarea by a logical point as its "worst-case" energy reception and energy consumption behavior.

- Based on the near-optimal solution to the idealized problem OPT-ub, we return to the original problem TPP by incorporating non-zero traveling time for the WCV. In particular, we determine the traveling path in TPP by finding the shortest Hamiltonian cycle to connect all the logical points that have

---

[1]A simpler version of bundling WPT and MBS problem was studied in [11], where the traveling path for the WCV was assumed to be given *a priori*. This assumption simplifies the problem considerably and the optimization problem only needs to find solutions to stopping points, charging schedule, and data flow routing. In contrast, this paper considers a much harder problem where the traveling path is unknown.

non-zero stopping time in OPT-ub. Note that this Hamiltonian cycle is fundamentally different from the Hamiltonian cycle that connects all sensor nodes in the network. Based on this traveling path, we can obtain a feasible solution to the original problem TPP. We further quantify the performance gap between this feasible solution and optimal solution to TPP.

The remainder of this paper is organized as follows. In Section 2, we give some essential background and necessary mathematical models for this problem. We also give a formulation for the optimization problem TPP. In Section 3, we study an idealized problem OPT-ub and develop a near-optimal solution. In Section 4, we determine a traveling path based on the solution in Section 3. From this path, we develop a feasible solution to the original problem TPP. We then quantify the performance gap between this solution and the optimal solution. Section 5 presents numerical results. Section 6 concludes this paper.

2. MODELING AND FORMULATION

Suppose that we have a sensor network $\mathcal{N}$ deployed over a two-dimensional area. A WCV is employed to recharge sensor nodes in the network and to collect data from nodes in real time. The WCV follows a periodic schedule: In each cycle, it starts from its home service station, travels inside the network, and returns to the service station. While traveling, the WCV makes a number of stops and charges sensor nodes that are in the vicinity of those stops (see Fig. 1). For the traveling path that we are investigating in this paper, the WCV is allowed to visit *anywhere* over the two-dimensional area, i.e., its traveling path is unconstrained and is part of the optimization problem. At any time, the data generated from the sensor nodes are relayed through multi-hops toward the WCV (in real time).

2.1 Traveling Path and Stopping Schedule

Denote $\mathcal{P}$ as the traveling path and τ as the amount of time for each cycle. Then τ includes three components:

- The total traveling time along path $\mathcal{P}$, $D_{\mathcal{P}}/V$, where $D_{\mathcal{P}}$ is the distance along path $\mathcal{P}$ and V is the traveling speed of the WCV.

- The total sojourn time along path $\mathcal{P}$, which is defined as the sum of all stopping time of the WCV when it travels on $\mathcal{P}$.

- The vacation time for the WCV at its home service station, τ_{vac}, which starts when the WCV returns to its home service station (after traveling path $\mathcal{P}$) and ends when the WCV leaves for the next trip.

Then we have:

$$\tau = \frac{D_{\mathcal{P}}}{V} + \sum_{p \in \mathcal{P}, \ p \neq p_{\text{vac}}}^{\omega(p)>0} \omega(p) + \tau_{\text{vac}} , \qquad (1)$$

where $\omega(p)$ denotes the aggregate amount of time the WCV stays at point $p \in \mathcal{P}$ and p_{vac} denotes the location of the home service station.

2.2 Energy Charging Model

We assume that the WCV can only perform its charging function when it makes a stop along path $\mathcal{P}$ (excluding p_{vac}). Based on the current charging technology [4, 10], the WCV can charge multiple neighboring nodes simultaneously as long as they are within its

charging range, although the power transfer rate at a sensor node decreases over the distance.

Denote $U_{iB}(p)$ as the power reception rate at node i when the WCV is located at $p \in \mathcal{P}$. Denote the efficiency of wireless charging by $\mu(D_{iB}(p))$, which is a decreasing function of $D_{iB}(p)$, the distance between node i and the WCV located at p. Then the wireless charging model is as follows [10]:

$$U_{iB}(p) = \begin{cases} \mu(D_{iB}(p)) \cdot U_{\max} & \text{if } D_{iB}(p) \leq D_\delta \\ 0 & \text{if } D_{iB}(p) > D_\delta , \end{cases} \quad (2)$$

where $U_{\max}$ is the maximum output power for a single sensor node and D_δ is the charging range of the WCV, beyond which wireless charging will not occur. In other words, D_δ is defined in a way such that the power reception rate at a sensor node is at least over a threshold value δ.

2.3 Dynamic Data Flow Routing

Recall that the base station is co-located at the WCV and all data generated from the sensor nodes shall be delivered to the base station. To conserve energy, multi-hop data routing is necessary among the sensor nodes in the network. Due to the mobility of the WCV, data flow routing is dynamic, with routing topology changing over time.

Suppose that each sensor node i ($i \in \mathcal{N}$) generates a constant rate R_i. Denote $f_{ij}(p)$ and $f_{iB}(p)$ as flow rates from sensor node i to sensor node j and to the base station when the WCV is at location $p \in \mathcal{P}$, respectively. Then we have the following flow balance at each sensor node i:

$$\sum_{k \in \mathcal{N}}^{k \neq i} f_{ki}(p) + R_i = \sum_{j \in \mathcal{N}}^{j \neq i} f_{ij}(p) + f_{iB}(p) \quad (i \in \mathcal{N}, p \in \mathcal{P}) \quad (3)$$

The above flow balance equation indicates that we are dealing with real-time flow routing, rather than DTN-like data routing (e.g., data MULEs [6] or message ferry [14]), where data can be delayed and delivered till a later time.

2.4 Sensor Energy Consumption

At a sensor node, we assume data communications (transmission and reception) is the dominant source for energy consumption.[2] Denote C_{ij} as the energy consumption rate for transmitting one unit of data flow from sensor node i to sensor node j. Then C_{ij} (in Joule/bit) can be modeled as [2, 7]:

$$C_{ij} = \beta_1 + \beta_2 D_{ij}^\alpha ,$$

where D_{ij} is the distance between nodes i and j, β_1 and β_2 are constant terms, and α is the path loss index. Given that all sensor nodes are stationary, we have that D_{ij} and C_{ij} are all constants.

Denote $C_{iB}(p)$ as the energy consumption rate for transmitting one unit of data flow from sensor node i to base station B when the WCV is at location $p \in \mathcal{P}$. We have

$$C_{iB}(p) = \beta_1 + \beta_2 \left[\sqrt{(x_p - x_i)^2 + (y_p - y_i)^2} \right]^\alpha , \quad (4)$$

where (x_p, y_p) and (x_i, y_i) are the coordinates of p and node i, respectively. Note that unlike C_{ij}'s, which are all constants, $C_{iB}(p)$ varies with the base station's position p.

---

[2]Energy consumption for hardware device and information processing can be assumed to be constants and can be easily integrated into total energy consumption without major change of the problem structure.

Then the total energy consumption rate for both transmission and reception at node i when the WCV is at $p \in \mathcal{P}$, denoted as $r_i(p)$, is

$$r_i(p) = \rho \sum_{k \in \mathcal{N}}^{k \neq i} f_{ki}(p) + \sum_{j \in \mathcal{N}}^{j \neq i} C_{ij} \cdot f_{ij}(p)$$
$$+ C_{iB}(p) \cdot f_{iB}(p) \quad (i \in \mathcal{N}, p \in \mathcal{P}) , \quad (5)$$

where ρ is a constant term associated with the rate of energy consumption for receiving one unit of data.

2.5 Energy Cycle at a Sensor Node

We will develop a travel schedule (including charging schedule) for the WCV and data flow routing among the nodes so that no sensor node ever runs out of energy. Such travel schedule follows a periodic cycle, as discussed in Section 2.1, with a cycle time of τ.

Suppose that each sensor node is fully charged initially. Denote $E_{\max}$ as its battery capacity and $E_{\min}$ as the minimum energy threshold for a node to be operational. We offer two energy renewable conditions, and show that once they are met, then the energy level at each sensor node at time t, denoted as $e_i(t)$, never falls below $E_{\min}$.

First, we split energy consumption at node i into two parts:

- Energy consumed whenever the WCV makes any stop (including vacationing at its service station): $r_i(p_{\text{vac}}) \cdot \tau_{\text{vac}} + \sum_{p \in \mathcal{P}, \ p \neq p_{\text{vac}}}^{\omega(p) > 0} r_i(p) \cdot \omega(p)$,

- Energy consumed when the WCV is moving along $\mathcal{P}$, i.e., $\int_{s \in [0, D_\mathcal{P}]}^{\omega(p(s)) = 0} \frac{1}{V} \cdot r_i(p(s)) \, ds$, where $s \in [0, D_\mathcal{P}]$ and the integration is taken over the distance traversed by the WCV along $\mathcal{P}$, and $p(s)$ is the WCV's location corresponding to s.

Following the results in [10], it can be shown that $e_i(t) \geq E_{\min}$ for all $t \geq 0$, $i \in \mathcal{N}$ if the following conditions are satisfied:

$$E_{\max} - \left[r_i(p_{\text{vac}}) \cdot \tau_{\text{vac}} + \sum_{p \in \mathcal{P}, \ p \neq p_{\text{vac}}}^{\omega(p) > 0, \ D_{iB}(p) > D_\delta} r_i(p) \cdot \omega(p) \right.$$
$$\left. + \int_{s \in [0, D_{\text{p}}]}^{\omega(p(s)) = 0} \frac{1}{V} \cdot r_i(p(s)) ds \right] \geq E_{\min} , \quad (i \in \mathcal{N}) \quad (6)$$

$$r_i(p_{\text{vac}}) \cdot \tau_{\text{vac}} + \sum_{p \in \mathcal{P}, \ p \neq p_{\text{vac}}}^{\omega(p) > 0} r_i(p) \cdot \omega(p)$$
$$+ \int_{s \in [0, D_{\text{p}}]}^{\omega(p(s)) = 0} \frac{1}{V} \cdot r_i(p(s)) ds$$
$$\leq \sum_{p \in \mathcal{P}}^{\omega(p) > 0, \ D_{iB}(p) \leq D_\delta} U_{iB}(p) \cdot \omega(p) , \quad (i \in \mathcal{N}) \quad (7)$$

In constraint (6), $\sum_{p \in \mathcal{P}, \ p \neq p_{\text{vac}}}^{\omega(p) > 0, \ D_{iB}(p) > D_\delta} r_i(p) \cdot \omega(p)$ is the amount of energy consumed at node i when the WCV is making stops near those nodes other than i. Constraint (6) ensures that $e_i(t)$, which starts from $E_{\max}$ at $t = 0$, will not fall below $E_{\min}$ at the end of the first cycle $t = \tau$. In constraint (7), the left hand side is the amount of energy consumed at node i during τ while the right hand side is maximum amount of potential energy received by node i in a cycle. Note that the actual amount of energy received by node i in the first cycle may be less than the right hand side due to battery overflow.[3] Constraint (7) ensures that $e_i(t)$, which starts at full level $E_{\max}$, will be charged back to $E_{\max}$ before the end of the first cycle τ.

2.6 Problem Formulation

Based on the above mathematical models, a number of problems can be formulated and studied. As a case study, we consider an optimization problem involving joint optimization of traveling path, stopping points, charging schedule, and flow routing. For the objective function, we consider minimizing energy consumption of the entire system, which includes power used by the WCV

---

[3]Once a battery is charged to $E_{\max}$, its energy cannot be further increased.

and the power consumed for wireless power transfer.[4] Since power used by the WCV is the dominant component in the overall energy consumption, our objective function will focus on this component. Specifically, we aim to minimize the fraction of time that the WCV is at work (i.e., away from its service station) in each cycle period, i.e., $\frac{D_{\mathcal{P}}/V + \sum_{p \in \mathcal{P}, \, p \neq p_{\mathrm{vac}}}^{\omega(p)>0} \omega(p)}{\tau}$.[5] Note that by (1), minimizing $\frac{D_{\mathcal{P}}/V + \sum_{p \in \mathcal{P}, \, p \neq p_{\mathrm{vac}}}^{\omega(p)>0} \omega(p)}{\tau}$ is equivalent to maximizing $\frac{\tau_{\mathrm{vac}}}{\tau}$, which is the percentage of time that the WCV is on vacation at its service station. Therefore, we have the following optimization problem.

TPP:

maximize $\frac{\tau_{\mathrm{vac}}}{\tau}$

s.t.   Time constraints: (1);
        Flow routing constraints: (3);
        Energy consumption model: (5);
        Energy renewable constraints: (6), (7).

$$\tau, \tau_{\mathrm{vac}}, \omega(p) \geq 0 \quad (p \in \mathcal{P})$$
$$f_{ij}(p), f_{iB}(p), r_i(p) \geq 0 \quad (i, j \in \mathcal{N}, i \neq j, p \in \mathcal{P}) .$$

In this formulation, V, R_i, ρ, C_{ij}, $E_{\max}$, and $E_{\min}$ are constants, and $U_{iB}(p)$ and $C_{iB}(p)$ can be computed by (2) and (4), respectively. The path $\mathcal{P}$ and $D_{\mathcal{P}}$ are to be determined in problem TPP. The time intervals τ, τ_{vac}, and $\omega(p)$, the flow rates $f_{ij}(p)$ and $f_{iB}(p)$, and the power consumption rate $r_i(p)$ are also optimization variables.[6] Note that problem TPP is a nonlinear program, and is NP-hard in general.

In problem TPP, the WCV can travel anywhere in the two-dimensional plane. It is not hard to see that the WCV's roaming area can be narrowed down to a much smaller area. In particular, it is sufficient for the WCV to roam in the smallest enclosing disk (SED) [9], denoted as $\mathcal{A}$, which covers all the sensor nodes in the network and the home service station. This result is stated in the following lemma.

LEMMA 1. *The optimal traveling path for the WCV must stay inside the SED $\mathcal{A}$.*

A proof sketch: A proof of this lemma can be easily constructed based on contradiction. That is, if there exists an optimal solution that involves the WCV traveling outside of the SED, we can always find a better solution (in terms of objective value) by bringing the WCV inside the SED, which leads to a contradiction. A formal proof is given in [12].

3. A NEAR-OPTIMAL SOLUTION TO AN IDEALIZED PROBLEM

A major difficulty in problem TPP is that the traveling path $\mathcal{P}$ is unknown and is part of the optimization problem. What further complicates this matter is that it takes time for the WCV to travel along the path. In this section, we consider an idealized problem

---

[4]Note that except their initial energy, the energy consumed at all sensor nodes comes from the WCV.

[5]We assume the WCV keeps its engine running as long as it is away from its service station.

[6]Note that variables in this formulation are only dependent on the WCV's location p and are independent of the time when the WCV visits this location. In [7], Shi *et al.* showed that a time-based formulation involving a MBS like ours can be transformed into a location-based formulation. In light of that result, we start directly with a location-based formulation in this paper without going through the details of such transformation, which are similar to those in [7].
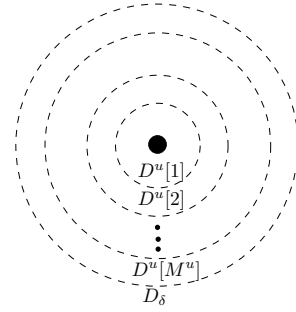
Figure 2: A sequence of circles centered at a node with decreasing energy charging rates.

that ignores the time for the WCV to travel from one point to another along $\mathcal{P}$. We will show that it is possible to develop a provably near-optimal solution to this idealized problem. Based on this result, in Section 4, we address the practical problem which considers non-zero traveling time for the WCV.

3.1 An Idealized Problem with Zero Traveling Time

In the idealized problem, the traveling time of the WCV is assumed to be zero. In this section, we give a formulation for this idealized problem (denoted as OPT-ub) based on our formulation for TPP. Since $V \to \infty$, constraint (1) becomes

$$\tau = \sum_{p \in \mathcal{P}, \, p \neq p_{\mathrm{vac}}}^{\omega(p)>0} \omega(p) + \tau_{\mathrm{vac}} . \tag{8}$$

Further, since $V \to \infty$ in OPT-ub, energy consumed at a sensor node i when the WCV travels along $\mathcal{P}$ (i.e., $\int_{s \in [0, D_{\mathrm{P}}]}^{\omega(p(s))=0} \frac{1}{V} \cdot r_i(p(s)) \, ds$) degenerates to 0. Hence, (7) can be simplified to

$$r_i(p_{\mathrm{vac}}) \cdot \tau_{\mathrm{vac}} + \sum_{p \in \mathcal{P}, \, p \neq p_{\mathrm{vac}}}^{\omega(p)>0} r_i(p) \cdot \omega(p)$$
$$\leq \sum_{p \in \mathcal{P}}^{\omega(p)>0, \, D_{iB}(p) \leq D_\delta} U_{iB}(p) \cdot \omega(p) \quad (i \in \mathcal{N}) , \tag{9}$$

and (6) can be simplified to

$$r_i(p_{\mathrm{vac}}) \cdot \tau_{\mathrm{vac}} + \sum_{p \in \mathcal{P}, \, p \neq p_{\mathrm{vac}}}^{\omega(p)>0, \, D_{iB}(p)>D_\delta} r_i(p) \cdot \omega(p)$$
$$\leq E_{\max} - E_{\min} \quad (i \in \mathcal{N}) . \tag{10}$$

Summarizing all these updates, OPT-ub can be written as follows:

OPT-ub:

maximize $\frac{\tau_{\mathrm{vac}}}{\tau}$

s.t.   Time constraints: (8);
        Flow routing constraints: (3);
        Energy consumption model: (5);
        Energy renewable constraints: (9), (10) .

$$\tau, \tau_{\mathrm{vac}}, \omega(p) \geq 0 \quad (p \in \mathcal{P})$$
$$f_{ij}(p), f_{iB}(p), r_i(p) \geq 0 \quad (i, j \in \mathcal{N}, i \neq j, p \in \mathcal{P}) .$$

Denote ψ_{TPP}^* and $\psi_{\mathrm{OPT\text{-}ub}}^*$ as an optimal solution to problem TPP and problem OPT-ub, respectively. Denote η_{TPP}^* as the objective value achieved by ψ_{TPP}^* and $\eta_{\mathrm{OPT\text{-}ub}}^*$ as the objective value achieved by $\psi_{\mathrm{OPT\text{-}ub}}^*$, respectively. The following lemma shows the relationship between $\eta_{\mathrm{OPT\text{-}ub}}^*$ and η_{TPP}^*.

LEMMA 2. $\eta_{OPT\text{-}ub}^*$ *is an upper bound of* η_{TPP}^**, i.e.,* $\eta_{OPT\text{-}ub}^* > \eta_{TPP}^*$*.*

A proof sketch: The proof of Lemma 2 can be constructed as follows. Suppose ψ_{TPP}^* is given. Then we can construct a solution

(a) Phase I. (b) Phase II. (c) Phase III.
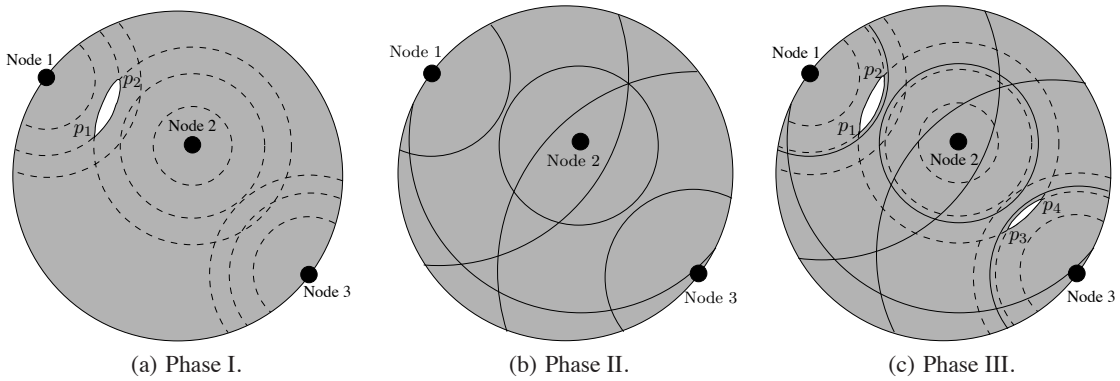
Figure 3: An example three-node sensor network illustrating area partition in three phases. The gray region is the SED of the three nodes.

$\psi_{\text{OPT-ub}}$ to problem OPT-ub with strictly greater objective value than η^*_{TPP}. Such construction of $\psi_{\text{OPT-ub}}$ is straightforward as OPT-ub is an ideal (or relaxed) case of TPP assuming zero traveling time. Since the obtained solution $\psi_{\text{OPT-ub}}$ is only feasible to OPT-ub, $\eta^*_{\text{OPT-ub}}$ (for $\psi^*_{\text{OPT-ub}}$) must be greater than η^*_{TPP}. A formal proof is given in [12].

In the rest of this section, we develop a near-optimal solution to OPT-ub. In Section 3.2, we partition the SED $\mathcal{A}$ into a number of smaller subareas. In Section 3.3, we employ the so-called *logical point* as a "worst-case" representation for each subarea in terms of energy reception and energy consumption. The logical point concept that we propose here generalizes the "fictitious cost point" proposed in [7], which only considered energy consumption. In Section 3.4, we propose an approximation algorithm to problem OPT-ub, and prove it near-optimality.

3.2 Area Partitioning

In this section, we partition the SED $\mathcal{A}$ into a number of smaller subareas. The partition is performed in a special way such that some lower and upper bounds can be derived regarding energy charging and consumption at each sensor node.

Phase I: Area Partition based on WPT. First, we discretize energy reception rate. Due to one-to-one mapping between distance and energy reception rate (see (2)), a discretization of energy reception rate also corresponds to a discretization of distance.

We discretize energy reception rates $U[1], U[2], \ldots, U[M^u]$ as follows:

$$U[h] = \begin{cases} U_{\max}(1 - \frac{\epsilon}{W})^h & \text{if } 0 \leq h \leq M^u \\ 0 & \text{otherwise} , \end{cases} \quad (11)$$

where M^u is the largest integer such that $U[M^u] > \delta$, ϵ is the allowed error margin for the near-optimal solution, W is a parameter controlling the granularity of the discretization (i.e., a large W leads to a large M^u).

Corresponding to $U[1], U[2], \ldots, U[M^u]$, we can discretize distance into $D^u[1], D^u[2], \ldots, D^u[M^u]$, and define $D^u[h]$ as follows:

$$D^u[h] = \mu^{-1}\left(\frac{U[h]}{U_{\max}}\right), \quad 1 \leq h \leq M^u ,$$

where $\mu^{-1}(\cdot)$ denotes the inverse function of (2).

To determine M^u, recall that M^u is the largest integer such that $U[M^u] > \delta$. By (11), we have

$$M^u = \left\lfloor \frac{\ln\left(\frac{\delta}{U_{\max}}\right)}{\ln\left(1 - \frac{\epsilon}{W}\right)} \right\rfloor . \quad (12)$$

For each node $i \in \mathcal{N}$, we draw M^u circles centered at node i, with each circle having an increasing radius $D^u[h], 1 \leq h \leq M^u$. Based on (2), there is a circle with a radius of D_δ that cuts off the charging area for node i. That is, when $D_{iB}(p) = D_\delta, U_{iB}(p) = \delta$ (see Fig. 2). Note that this last cut-off circle, along with the M^u-th inner circle (i.e. the second outermost circle) partition $\mathcal{A}$ into three regions:

(i). A disk with a radius of $D^u[M^u]$, where $U[M^u] \leq U_{iB}(p) \leq U_{\max}$.

(ii). A ring bounded by these two circles with radiuses of $D^u[M^u]$ and D_δ, respectively, where $\delta \leq U_{iB}(p) < U[M^u]$.

(iii). The area outside of the cut-off circle, in which $U_{iB}(p) = 0$.

Since we have $(M^u + 1)$ circles for each node i, the intersections of these circles partition disk $\mathcal{A}$ into a number of irregular subareas. As an example, for the 3-node network in Fig. 3(a), suppose that $M^u = 2$. Then we draw 3 circles for each node. Disk $\mathcal{A}$ in Fig. 3(a) is partitioned into 19 irregular subareas. For the subarea of white color with corner points p_1 and p_2, any point p in this subarea satisfies $U[2] \leq U_{1B}(p) \leq U[1]$ with respect to node 1. With respect to nodes 2 and 3, for any point p in this same subarea, we have $\delta \leq U_{2B}(p) \leq U[2]$, and $U_{3B}(p) = 0$.

As shown in the example, the proposed area partition gives tight lower and upper bounds for each subarea. In particular, for a subarea $\mathcal{A}^u$ with $D_{iB}(p) \leq D^u[M^u]$ where $p \in \mathcal{A}^u$, we have

$$U[h_i^u(\mathcal{A}^u)] \leq U_{iB}(p) \leq U[h_i^u(\mathcal{A}^u) - 1] , \ p \in \mathcal{A}^u , \quad (13)$$

where $h_i^u(\mathcal{A}^u)$ denotes the index of the outer circle (centered at node i), and $h_i^u(\mathcal{A}^u) \leq M^u$. For a given subarea $\mathcal{A}^u$, $h_i^u(\mathcal{A}^u)$ can be determined by (11) and (13). We have

$$h_i^u(\mathcal{A}^u) = \left\lceil \frac{\ln\left(U_{iB}(p)/U_{\max}\right)}{\ln\left(1 - \epsilon/W\right)} \right\rceil , \ p \in \mathcal{A}^u , \quad (14)$$

Therefore, for any $p \in \mathcal{A}^u$, we have the lower bound for energy reception $U_{iB}(p)$ as follows:

$$U[h_i^u(\mathcal{A}^u)] = \begin{cases} U_{\max}(1 - \frac{\epsilon}{W})^{h_i^u(\mathcal{A}^u)}, & \text{if } D_{iB}(p) \leq D^u[M^u], \\ \delta, & \text{if } D^u[M^u] < D_{iB}(p) \leq D_\delta, \\ 0, & \text{otherwise.} \end{cases}$$

$$(15)$$

where $h_i^u(\mathcal{A}^u)$ is determined by (14).

Phase II: Area Partition based on Energy Consumption. Following a similar token to that in Phase I, we discretize energy consumption rate, which also corresponds to a discretization of dis-

tance. Specifically, for each node $i \in \mathcal{N}$, we define a sequence of increasing energy costs $C[1], C[2], \ldots, C[M_i^c]$ as follows:

$$C[h] = \beta_1 \left(1 + \frac{\epsilon}{W}\right)^h , \qquad (16)$$

where M_i^c is the largest number of elements in the sequence of $C[h]$. Corresponding to $C[h]$, $h = 1, 2, \ldots, M_i^c$, we can discretize distance into $D^c[1], D^c[2], \ldots, D^c[M_i^c]$, where

$$D^c[h] = \left(\frac{C[h] - \beta_1}{\beta_2}\right)^{-\alpha} , \quad 0 \le h \le M_i^c + 1 .$$

For each node $i \in \mathcal{N}$, we can draw M_i^c circles centered at node i, with increasing radii $D^c[1], D^c[2], \ldots, D^c[M_i^c]$. To determine M_i^c, denote $O_{\mathcal{A}}$ and $R_{\mathcal{A}}$ as the origin and radius of $\mathcal{A}$, respectively. Denote $D_{i,O_{\mathcal{A}}}$ as the distance from node i to $O_{\mathcal{A}}$. As $D_{iB}(p) \in [0, D_{i,O_{\mathcal{A}}} + R_{\mathcal{A}}]$, by (4), we have $C_{iB} \in [\beta_1, \beta_1 + \beta_2 \cdot (D_{i,O_{\mathcal{A}}} + R_{\mathcal{A}})^\alpha]$. Since the WCV can only travel within $\mathcal{A}$, M_i^c is the largest integer such that $C[M_i^c] < \beta_1 + \beta_2 \cdot (D_{i,O_{\mathcal{A}}} + R_{\mathcal{A}})^\alpha$. By (16), we have

$$M_i^c = \left\lfloor \frac{\ln\left(1 + \frac{\beta_2}{\beta_1} \cdot (D_{i,O_{\mathcal{A}}} + R_{\mathcal{A}})^\alpha\right)}{\ln\left(1 + \frac{\epsilon}{W}\right)} \right\rfloor .$$

Since we have M_i^c circles for $i \in \mathcal{N}$, the intersections of these circles partition $\mathcal{A}$ into a number of subareas (see Fig. 3(b)). For a subarea $\mathcal{A}^c$, we have

$$C[h_i^c(\mathcal{A}^c) - 1] \le C_{iB}(p) \le C[h_i^c(\mathcal{A}^c)] , \quad p \in \mathcal{A}^c , \qquad (17)$$

where $h_i^c(\mathcal{A}^c)$ denotes the index of the outer circle (centered at node i) that contains $\mathcal{A}^c$. Given a subarea $\mathcal{A}^c$, $h_i^c(\mathcal{A}^c)$ can be determined by (16) and (17). Thus, we have

$$h_i^c(\mathcal{A}^c) = \left\lceil \frac{\ln\left(1 + \frac{\beta_2}{\beta_1} \cdot D_{iB}(p)^\alpha\right)}{\ln\left(1 + \frac{\epsilon}{W}\right)} \right\rceil . \qquad (18)$$

Therefore, for any $p \in \mathcal{A}^c$, a tight upper bound of $C_{iB}(p)$ is:

$$C[h_i^c(\mathcal{A}^c)] = \beta_1 \left(1 + \frac{\epsilon}{W}\right)^{h_i^c(\mathcal{A}^c)} , \qquad (19)$$

where $h_i^c(\mathcal{A}^c)$ is determined by (18).

Phase III: Joint Area Partition. By combining the partitions in both Phases I and II, the disk $\mathcal{A}$ is partitioned into smaller subareas $\mathcal{A}_k^{u+c}$, $k = 1, 2, \ldots, K$ (see Fig. 3(c)). For each subarea $\mathcal{A}_k^{u+c}$, both the energy reception and consumption can be tightly bounded.

Now we give an upper bound on the number of subareas K. By (12), we have

$$M^u = \left\lfloor \frac{\ln\left(\frac{\delta}{U_{\max}}\right)}{\ln\left(1 - \frac{\epsilon}{W}\right)} \right\rfloor = O\left(\left\lfloor \frac{1}{\frac{\epsilon}{W}} \right\rfloor\right) = O\left(\frac{W}{\epsilon}\right) ,$$

where the second equality holds since $\ln\left(\delta/U_{\max}\right)$ is a negative constant and $\ln(1 - \epsilon/W) \approx -\epsilon/W$ for small ϵ/W. Similarly, we have

$$\begin{aligned}
M_i^c &= \left\lfloor \frac{\ln\left(1 + \frac{\beta_2}{\beta_1} \cdot (D_{i,O_{\mathcal{A}}} + R_{\mathcal{A}})^\alpha\right)}{\ln\left(1 + \frac{\epsilon}{W}\right)} \right\rfloor \\
&= O\left(\left\lfloor \frac{1}{\frac{\epsilon}{W}} \right\rfloor\right) = O\left(\frac{W}{\epsilon}\right) .
\end{aligned}$$

For each sensor node, there are $(M^u + 1)$ circles from Phase I and M_i^c circles from Phase II. Putting these circles and one more circle for $\mathcal{A}$ together, the total number of circles is $B = 1 + \sum_{i \in \mathcal{N}} (M^u + M_i^c + 1)$. Given B circles, the maximum number of subareas K is

upper bounded by $K \le B^2 - B + 2$ (which can be easily verified by induction). That is

$$\begin{aligned}
K = O(B^2) &= O\left(\left[1 + \sum_{i \in \mathcal{N}} (M^u + M_i^c + 1)\right]^2\right) \\
&= O\left(\left(\frac{W|\mathcal{N}|}{\epsilon}\right)^2\right) . \qquad (20)
\end{aligned}$$

3.3 Logical Point Representation

For each subarea $\mathcal{A}_k^{u+c}$, $k = 1, 2, \ldots, K$, we represent it as a *logical point* $\mathcal{L}_k$. Denote $\omega(\mathcal{L}_k)$ as the total stopping time when the WCV is in subarea $\mathcal{A}_k^{u+c}$. Then we have,

$$\omega(\mathcal{L}_k) = \sum_{p \in \mathcal{A}_k^{u+c}}^{\omega(p) > 0} \omega(p) .$$

To characterize a logical point $\mathcal{L}_k$, we use the worst case bounds of energy charging and energy consumption rates within the subarea $\mathcal{A}_k^{u+c}$. Specifically, for a logical point $\mathcal{L}_k$, we use a $|2\mathcal{N}|$-tuple to represent a logical point, where the first $|\mathcal{N}|$ components are for energy charging and the other $|\mathcal{N}|$ components are for energy consumption, i.e., $\left[U_1(\mathcal{L}_k), U_2(\mathcal{L}_k), \ldots, U_{|\mathcal{N}|}(\mathcal{L}_k), C_{1B}(\mathcal{L}_k), C_{2B}(\mathcal{L}_k), \ldots, C_{|\mathcal{N}|B}(\mathcal{L}_k)\right]$. In this vector, the first $|\mathcal{N}|$ components are

$$U_i(\mathcal{L}_k) = U[h_i^u(\mathcal{A}_k^{u+c})] , \qquad (21)$$

where $U[h_i^u(\mathcal{A}_k^{u+c})]$ is the lower bound of $U_{iB}(p)$ for any $p \in \mathcal{A}_k^{u+c}$ and is determined by (15), while the next $|\mathcal{N}|$ components are

$$C_{iB}(\mathcal{L}_k) = C[h_i^c(\mathcal{A}_k^{u+c})] , \qquad (22)$$

where $C[h_i^c(\mathcal{A}_k^{u+c})]$ is the upper bound of $C_{iB}(p)$ for any $p \in \mathcal{A}_k^{u+c}$ and is determined by (19).

3.4 A Near-Optimal Solution

Based on these logical points, we can develop a provably near-optimal solution to problem OPT-ub. Recall that $\psi^*_{\text{OPT-ub}}$ is an optimal solution to problem OPT-ub, and $\eta^*_{\text{OPT-ub}}$ is the objective value achieved by $\psi^*_{\text{OPT-ub}}$. Our goal is to find a feasible solution to problem OPT-ub, denoted as $\psi_{\text{OPT-ub}}$, so that $\eta_{\text{OPT-ub}} \ge \eta^*_{\text{OPT-ub}} - \epsilon$.

A Worst-Case Formulation and Its Solution. Note that a logical point is a worst-case representation of the subarea in terms of energy charging and energy consumption. Based on these logical points, we can have a formulation, denoted as OPT-$\mathcal{L}$, that can be used to derive a lower bound to OPT-ub. Problems OPT-$\mathcal{L}$ and OPT-ub are similar to each other except the following differences:

- OPT-$\mathcal{L}$ is based on a finite number of logical points while OPT-ub is based on an infinite number of physical points.

- For $p \neq p_{\text{vac}}$, we have $\omega(\mathcal{L}_k), f_{ij}(\mathcal{L}_k), f_{iB}(\mathcal{L}_k), r_i(\mathcal{L}_k)$ in OPT-$\mathcal{L}$ rather than $\omega(p), f_{ij}(p), f_{iB}(p), r_i(p)$ in OPT-ub.

- We have $U_i(\mathcal{L}_k)$ and $C_{iB}(\mathcal{L}_k)$ in OPT-$\mathcal{L}$ rather than $U_i(p)$ and $C_{iB}(p)$ in OPT-ub.

Through a number of changes of variables, OPT-$\mathcal{L}$ can be reformulated into a linear program (LP), which can be solved in polynomial time (see Appendix A for more details).

Recover a Feasible Solution to OPT-ub. After we obtain an optimal solution to problem OPT-$\mathcal{L}$, denoted as $\psi_{\text{OPT-}\mathcal{L}}$, we need

to recover a solution to OPT-ub (denoted by $\psi_{\text{OPT-ub}}$). Suppose that $\psi_{\text{OPT-ub}} = (\tau, \tau_{\text{vac}}, \omega(p), f_{ij}(p), f_{iB}(p), r_i(p))$. From $\psi_{\text{OPT-}\mathcal{L}}$, $\psi_{\text{OPT-ub}}$ can be constructed as follows:

- τ and τ_{vac} are the same as their counterparts in $\psi_{\text{OPT-}\mathcal{L}}$.
- For $p = p_{\text{vac}}$, $f_{ij}(p_{\text{vac}})$, $f_{iB}(p_{\text{vac}})$, $r_i(p_{\text{vac}})$ are the same as their counterparts in $\psi_{\text{OPT-}\mathcal{L}}$.
- For any $\omega(\mathcal{L}_k) > 0$, choose a point $p_k \in \mathcal{A}_k^{u+c}$ and set $\omega(p_k) = \omega(\mathcal{L}_k)$. Further, set flow routing $f_{ij}(p_k) = f_{ij}(\mathcal{L}_k)$ and $f_{iB}(p_k) = f_{iB}(\mathcal{L}_k)$. Determine $r_i(p_k)$ by (5).

Denote $\eta_{\text{OPT-}\mathcal{L}}$ and $\eta_{\text{OPT-ub}}$ as the objective values achieved by $\psi_{\text{OPT-}\mathcal{L}}$ and $\psi_{\text{OPT-ub}}$, respectively. Since τ and τ_{vac} are unchanged in the foregoing solution construction, we have

$$\eta_{\text{OPT-ub}} = \eta_{\text{OPT-}\mathcal{L}} \ . \tag{23}$$

The following lemma affirms the feasibility of the constructed solution $\psi_{\text{OPT-ub}}$ to problem OPT-ub.

LEMMA 3. *$\psi_{\text{OPT-ub}}$ is a feasible solution to problem OPT-ub.*

A proof of Lemma 3 is given in Appendix B.

Proof of Near-Optimality. The near-optimality of $\psi_{\text{OPT-ub}}$ is stated in the following theorem.

THEOREM 1. *For a given $\epsilon > 0$, $\eta_{\text{OPT-ub}} \geq \eta^*_{\text{OPT-ub}} - \epsilon$.*

A proof sketch: Theorem 1 can be proved based on solution construction. First, we show that given a feasible solution $\hat{\psi}_{\text{OPT-ub}}$ to OPT-ub with an objective value $\hat{\eta}_{\text{OPT-ub}}$, we can construct a solution $\hat{\psi}_{\text{OPT-}\mathcal{L}}$ to OPT-$\mathcal{L}$ with an objective value $\hat{\eta}_{\text{OPT-}\mathcal{L}} \geq \hat{\eta}_{\text{OPT-ub}} - \epsilon$. Second, we consider a special case that the given solution $\hat{\psi}_{\text{OPT-ub}}$ is an optimal solution $\psi^*_{\text{OPT-ub}}$ to OPT-ub with an objective value $\eta^*_{\text{OPT-ub}}$. Based on this construction, we can obtain a solution to OPT-$\mathcal{L}$ with an objective value at least $\eta^*_{\text{OPT-ub}} - \epsilon$. Since this solution is only a feasible solution to OPT-$\mathcal{L}$ while $\psi_{\text{OPT-}\mathcal{L}}$ is an optimal solution, we have $\eta_{\text{OPT-}\mathcal{L}} \geq \eta^*_{\text{OPT-ub}} - \epsilon$. Further, we have $\eta_{\text{OPT-ub}} = \eta_{\text{OPT-}\mathcal{L}} \geq \eta^*_{\text{OPT-ub}} - \epsilon$, where the first equality holds by (23).

4. A PRACTICAL SOLUTION AND PERFORMANCE GAP ANALYSIS

In Section 3, we have developed a near-optimal solution to an idealized problem, in which a WCV's traveling time is assumed to be zero. In this section, we incorporate traveling time and develop a practical solution to our original problem (TPP). We also quantify the performance gap between this solution and optimal (unknown) solution to TPP.

4.1 Fixing a Traveling Path

The near-optimal solution $\psi_{\text{OPT-ub}}$ to the idealized problem OPT-ub in Section 3 offers us several tools in designing a solution to the original problem TPP. First, the objective value $\eta_{\text{OPT-ub}}$ of $\psi_{\text{OPT-ub}}$ is at least $\eta^*_{\text{OPT-ub}} - \epsilon$ while $\eta^*_{\text{OPT-ub}}$ is an upper bound for the unknown objective value η^*_{TPP} of TPP. This can be used as a performance benchmark to measure the quality of the practical solution (which includes traveling time) to the original problem TPP. Second, the logical point concept in the near-optimal solution $\psi_{\text{OPT-ub}}$ offers a hint on where the WCV should make stops and charge the sensor nodes. We will exploit these stops in $\psi_{\text{OPT-ub}}$ to design a solution to problem TPP.

For the stopping points (any physical point within a logical point that has non-zero stopping time) in $\psi_{\text{OPT-ub}}$, we propose to find a
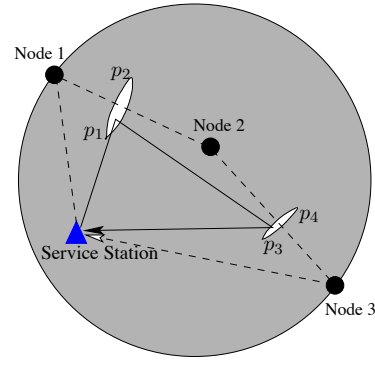

Figure 4: **Comparison between a Hamiltonian cycle connecting the logical points and the service station and a Hamiltonian cycle connecting the sensor nodes and the service station.**

shortest Hamiltonian cycle to connect them. Note that the service station is also included in this shortest Hamiltonian cycle. Denote this path by $\mathcal{P}_{\text{OPT-lb}}$. The decision of using shortest Hamiltonian cycle is obvious as it corresponds to the least amount of traveling time (not including stopping time).

It is important to realize that the shortest Hamiltonian cycle that we find here is based on the connection of logical points, rather than the actual sensor nodes. A Hamiltonian cycle for the latter would be fundamentally different from the former. As an example, in Fig. 4, the solid triangle is a Hamiltonian cycle connecting two logical points (with corner points (p_1, p_2) and (p_3, p_4)) and the service station while the dotted quadrangle is a Hamiltonian cycle connecting three sensor nodes and the service station.

4.2 Incorporating Traveling Time

Under the selected traveling path $\mathcal{P}_{\text{OPT-lb}}$, denote G as the total number of physical points with positive stopping time. We re-index these points by traveling order under $\mathcal{P}_{\text{OPT-lb}}$, and let $\mathcal{P}_{\text{OPT-lb}} = (p_{\text{vac}}, p_1, \ldots, p_G, p_{\text{vac}})$, with the starting and ending point being the service station (p_{vac}) and the j-th stop along the path being p_j, $1 \leq j \leq G$.

To find flow routing when the WCV travels along $\mathcal{P}_{\text{OPT-lb}}$, we discretize $\mathcal{P}_{\text{OPT-lb}}$ into a sequence of segments based on $\mathcal{P}_{\text{OPT-lb}}$'s intersection with the subareas (see Figs. 3(c) and 4). Based on this path discretization, we can rewrite TPP into a new formulation (denoted as OPT-lb), in which we can obtain flow routing when the WCV is traveling on each segment along path $\mathcal{P}_{\text{OPT-lb}}$.

Note that each segment is contained by one subarea. Among these traversed subareas, the WCV makes stops at some of them while only traversing others without making any stop. Denote $\mathcal{Q}$ as the set of indexes for all the traversed subareas and $\mathcal{Q}_s$ as the set of indexes for those subareas that the WCV makes stops, respectively. For $m \in \mathcal{Q}$, the WCV's traveling time (not including stopping time) in this subarea is $D(\mathcal{L}_m)/V$, where $\mathcal{L}_m$ is the logical point corresponding to this subarea, and $D(\mathcal{L}_m)$ denotes the distance traversed within $\mathcal{L}_m$ along $\mathcal{P}_{\text{OPT-lb}}$.

For $m \in \mathcal{Q}_s$, since the WCV makes a stop only at one point, we have $|\mathcal{Q}_s| = G$. The total time that the WCV spends in $\mathcal{L}_m$ is

$$\frac{D(\mathcal{L}_m)}{V} + \omega(\mathcal{L}_m) \ ,$$

where $\omega(\mathcal{L}_m)$ is the stopping time within $\mathcal{L}_m$. Based on $\mathcal{P}_{\text{OPT-lb}}$ and $\mathcal{L}_m, m \in \mathcal{Q}$, we rewrite problem TPP to OPT-lb as follows:

OPT-lb

maximize $\frac{\tau_{vac}}{\tau}$

s.t. $\tau = \tau_{vac} + \sum_{m \in \mathcal{Q}_s} \omega(\mathcal{L}_m) + \sum_{m \in \mathcal{Q}} \frac{D(\mathcal{L}_m)}{V}$ (24)

$\sum_{k \in \mathcal{N}}^{k \neq i} f_{ki}(\mathcal{L}_m) + R_i = \sum_{j \in \mathcal{N}}^{j \neq i} f_{ij}(\mathcal{L}_m) + f_{iB}(\mathcal{L}_m)$
$(i \in \mathcal{N}, m \in \mathcal{Q})$

$r_i(\mathcal{L}_m) = \rho \sum_{k \in \mathcal{N}}^{k \neq i} f_{ki}(\mathcal{L}_m) + \sum_{j \in \mathcal{N}}^{j \neq i} C_{ij} \cdot f_{ij}(\mathcal{L}_m)$
$\qquad + C_{iB}(\mathcal{L}_m) \cdot f_{iB}(\mathcal{L}_m) \quad (i \in \mathcal{N}, m \in \mathcal{Q})$

$r_i(p_{vac}) \cdot \tau_{vac} + \sum_{m \in \mathcal{Q}_s} r_i(\mathcal{L}_m) \cdot \omega(\mathcal{L}_m)$
$\qquad + \sum_{m \in \mathcal{Q}} \frac{D(\mathcal{L}_m)}{V} \cdot r_i(\mathcal{L}_m)$
$\qquad \leq \sum_{m \in \mathcal{Q}_s}^{D_{iB}(p) \leq D_\delta, p \in \mathcal{A}_m^{u+c}} U_{iB}(\mathcal{L}_m) \cdot \omega(\mathcal{L}_m) \quad (i \in \mathcal{N})$ (25)

$r_i(p_{vac}) \cdot \tau_{vac} + \sum_{m \in \mathcal{Q}_s}^{D_{iB}(p) > D_\delta, p \in \mathcal{A}_m^{u+c}} r_i(\mathcal{L}_m) \cdot \omega(\mathcal{L}_m)$
$\qquad + \sum_{m \in \mathcal{Q}} \frac{D(\mathcal{L}_m)}{V} \cdot r_i(\mathcal{L}_m) \leq E_{max} - E_{min} \quad (i \in \mathcal{N})$ (26)

$\tau, \tau_{vac}, \omega(\mathcal{L}_m) \geq 0 \quad (m \in \mathcal{Q}_s)$

$f_{ij}(\mathcal{L}_m), f_{iB}(\mathcal{L}_m), r_i(\mathcal{L}_m) \geq 0 \quad (i, j \in \mathcal{N}, i \neq j, m \in \mathcal{Q})$

$f_{ij}(p_{vac}), f_{iB}(p_{vac}), r_i(p_{vac}) \geq 0 \quad (i, j \in \mathcal{N}, i \neq j)$

In problem OPT-lb, time constraint (24) incorporates traveling time along $\mathcal{P}_{OPT\text{-}lb}$. Also, constraints (25) and (26) incorporate energy consumption when the WCV is traveling.

Through a similar change-of-variable procedure to that in Appendix A for OPT-$\mathcal{L}$, we can reformulate OPT-lb to an LP. By solving this LP, we can obtain a feasible solution to problem TPP. Denote $\psi_{OPT\text{-}lb}$ as this feasible solution and $\eta_{OPT\text{-}lb}$ as the objective value achieved by $\psi_{OPT\text{-}lb}$. The relationship between $\eta_{OPT\text{-}lb}$ and the optimum objective value η_{TPP}^* is given in the following lemma.

LEMMA 4. $\eta_{OPT\text{-}lb}$ *is a lower bound of* η_{TPP}^*, *i.e.,* $\eta_{OPT\text{-}lb} \leq \eta_{TPP}^*$.

Clearly, Lemma 4 holds since OPT-lb is based on a specified path $\mathcal{P}_{OPT\text{-}lb}$ and thus $\psi_{OPT\text{-}lb}$ is only a feasible solution to problem TPP.

4.3 Analysis of Performance Gap and Algorithm Complexity

Denote θ as the performance gap between $\eta_{OPT\text{-}lb}$ and the unknown optimal objective η_{TPP}^*. We have the following lemma.

LEMMA 5. $\theta \leq \epsilon + \eta_{OPT\text{-}ub} - \eta_{OPT\text{-}lb}$.

PROOF. By definition, $\theta = \eta_{TPP}^* - \eta_{OPT\text{-}lb}$, we have

$$\theta \leq \eta_{OPT\text{-}ub}^* - \eta_{OPT\text{-}lb} \leq \epsilon + \eta_{OPT\text{-}ub} - \eta_{OPT\text{-}lb} ,$$

where the first inequality holds by Lemma 2, and the second inequality holds by Theorem 1. □

In the above solution, solving two LPs (i.e., problems OPT-$\mathcal{L}$ and OPT-lb) has the highest complexity. The problem size of either LP is decided by the maximum number of subareas, which is a polynomial in $|\mathcal{N}|$ (see (20)). Thus, both LPs have polynomial size and the algorithm complexity is polynomial.

5. NUMERICAL RESULTS

Network and Parameter Settings. In the numerical results, the units of distance, time, data rate, and energy are all normalized appropriately. We assume sensor nodes are randomly deployed over a unit square area. The data rate R_i, $i \in \mathcal{N}$, is randomly generated within $[0.1, 1]$. The home service station is assumed to be at $(0.5, 0.5)$, and the WCV travels at a speed $V = 0.1$.

Table 1: Location and data rate R_i for each node in a 50-node network.

Node Index	Location	R_i	Node Index	Location	R_i
1	(0.547,0.644)	0.1	26	(0.833,0.115)	0.2
2	(0.662,0.757)	0.7	27	(0.639,0.658)	0.1
3	(0.037,0.859)	0.4	28	(0.704,0.930)	0.6
4	(0.723,0.741)	1.0	29	(0.977,0.306)	0.8
5	(0.529,0.778)	0.9	30	(0.673,0.386)	0.5
6	(0.316,0.035)	0.4	31	(0.021,0.745)	0.7
7	(0.190,0.842)	0.8	32	(0.924,0.072)	0.6
8	(0.288,0.106)	0.8	33	(0.270,0.829)	0.1
9	(0.040,0.942)	0.2	34	(0.777,0.573)	0.8
10	(0.264,0.648)	0.4	35	(0.097,0.512)	0.9
11	(0.446,0.805)	0.5	36	(0.986,0.290)	0.2
12	(0.890,0.729)	0.5	37	(0.161,0.636)	0.7
13	(0.370,0.350)	0.1	38	(0.355,0.767)	0.9
14	(0.006,0.101)	0.7	39	(0.655,0.574)	0.5
15	(0.393,0.548)	0.1	40	(0.031,0.052)	0.4
16	(0.629,0.623)	0.1	41	(0.350,0.150)	0.3
17	(0.084,0.954)	0.5	42	(0.941,0.724)	0.1
18	(0.756,0.840)	0.2	43	(0.966,0.430)	0.2
19	(0.966,0.376)	0.7	44	(0.107,0.191)	0.3
20	(0.931,0.308)	0.6	45	(0.007,0.337)	0.3
21	(0.944,0.439)	0.1	46	(0.457,0.287)	0.4
22	(0.626,0.323)	0.4	47	(0.753,0.383)	0.1
23	(0.537,0.538)	0.2	48	(0.945,0.909)	0.1
24	(0.118,0.082)	0.3	49	(0.209,0.758)	0.3
25	(0.929,0.541)	0.2	50	(0.221,0.588)	0.8

Table 2: Index of stopping points along the path, location and stopping time at each stopping point for the 50-node network.

| Stopping point	Location	τ_k	Stopping point	Location	τ_k
1	(0.575,0.550)	0.3	18	(0.525,0.775)	179.3
2	(0.600,0.575)	77.2	19	(0.375,0.775)	69.8
3	(0.750,0.575)	179.4	20	(0.350,0.775)	117.9
4	(0.675,0.375)	50.9	21	(0.200,0.825)	175.9
5	(0.650,0.350)	66.2	22	(0.075,0.950)	110.0
6	(0.900,0.075)	98.6	23	(0.025,0.775)	166.6
7	(0.925,0.075)	38.8	24	(0.025,0.750)	3.1
8	(0.975,0.300)	12.2	25	(0.200,0.625)	86.5
9	(0.975,0.325)	81.8	26	(0.225,0.625)	43.5
10	(0.975,0.350)	102.9	27	(0.150,0.550)	136.8
11	(0.925,0.525)	42.3	28	(0.100,0.525)	105.1
12	(0.900,0.725)	103.6	29	(0.000,0.325)	64.7
13	(0.950,0.900)	21.8	30	(0.000,0.100)	26.4
14	(0.700,0.925)	124.2	31	(0.050,0.125)	180.6
15	(0.725,0.750)	160.6	32	(0.300,0.100)	173.3
16	(0.700,0.750)	32.4	33	(0.450,0.300)	84.3
17	(0.675,0.750)	18.9	34	(0.400,0.550)	19.8
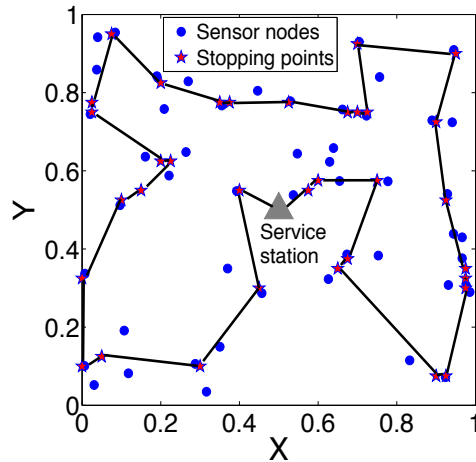
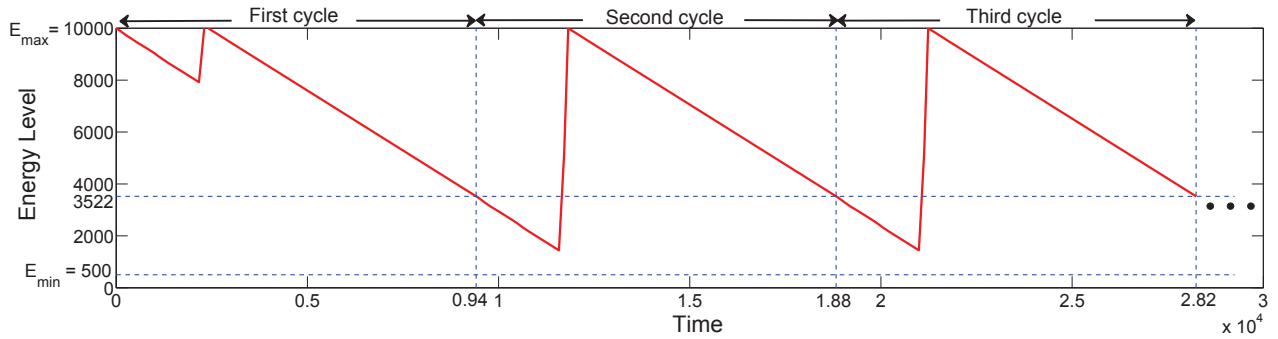**Figure 5: A traveling path for the WCV in the 50-node sensor network.**

Figure 6: The energy behavior of the 35th sensor node in the 50-node network during the first three cycles.

Suppose that a sensor node uses a rechargeable battery with $E_{max} = 10,000$, and $E_{min} = 500$. For the charging efficiency function $\mu(D_{iB})$, we assume a decreasing function $\mu(D_{iB}) = -40 \cdot D_{iB}^2 - 4 \cdot D_{iB} + 1.0$. Letting $U_{max} = 50$ and $\delta = 10$, we have $D_\delta = 0.10$ for a maximum distance of effective charging. The normalized parameters in energy consumption model are $\beta_1 = \beta_2 = \rho = 1$. The path loss index is $\alpha = 4$. We set $W = 3$ and $\epsilon = 0.05$ for the numerical results.

We consider a 50-node network. The normalized location of each node and its data rate are given in Table 1.

Results. Table 2 gives the stopping points (each within a logical point with a non-zero stopping time) along the travel path for the WCV. The traveling path is shown in Fig. 5. For $\mathcal{P}_{OPT\text{-}lb}$, $D_{\mathcal{P}_{OPT\text{-}lb}} = 4.89$ and the traveling time $D_{\mathcal{P}_{OPT\text{-}lb}}/V = 48.9$. Table 2 shows the charging schedule at each stopping point on $\mathcal{P}_{OPT\text{-}lb}$. Following $\mathcal{P}_{OPT\text{-}lb}$ and this charging schedule, our solution ensures that any sensor node never runs out of energy. As an example, Fig. 6 shows the energy behavior of a sensor node (the 35th node) during the first three cycles. During each cycle, this node is charged by the WCV when it makes stops at two stopping points (i.e., the 27th and 28th points). Starting from the second cycle, the node's energy behavior repeats from cycle to cycle.

For the given $\epsilon = 0.05$, we have $\eta_{OPT\text{-}ub} = 68.62\%$. For the obtained practical solution $\psi_{OPT\text{-}lb}$, the cycle time $\tau = 9414$, the vacation time $\tau_{vac} = 6410$, and the objective value is $\eta_{OPT\text{-}lb} = 68.09\%$. By Lemma 5, the performance gap $\theta \le \epsilon + \eta_{OPT\text{-}ub} - \eta_{OPT\text{-}lb} = 0.05 + 0.6862 - 0.6809 = 0.0553$, where the given ϵ is the dominant part. This shows that the objective value by the lower bound feasible solution is very close to that by the upper bound solution.

6. CONCLUSIONS

In this paper, we studied the problem of co-locating the MBS on the WCV in a WSN, with a focus on the traveling path problem of the WCV. The goal was to minimize energy consumption of the the entire system while ensuring none of the sensor nodes runs out of energy. We formulated an optimization problem (TPP) that involved joint optimization of traveling path, stopping points, charging schedule, and data flow routing. We first considered an idealized problem (OPT-ub) that assumed zero traveling time. For OPT-ub, we developed a provably near-optimal solution which involves several novel techniques, such as discretization of energy reception rate and energy consumption rate, double partitioning of the SED into smaller subareas with tight energy bounds, and representation of each subarea by a logical point as its "worst-case" energy reception and consumption behavior. Based on the near-optimal solution to the idealized problem OPT-ub, we set the trav-

eling path as the shortest Hamiltonian cycle connecting the logical points and the service station. We then obtained a practical solution (with non-zero traveling time) to the original problem TPP, and quantified the performance gap between this feasible solution and an optimal (unknown) solution to TPP.

7. ACKNOWLEDGMENTS

8. REFERENCES

[1] S. Basagni, A. Carosi, C. Petrioli, and C.A. Phillips. Coordinated and controlled mobility of multiple sinks for maximizing the lifetime of wireless sensor networks. *Springer Wirel. Netw.*, 17(3): 759–778, Apr. 2011.

[2] Y.T. Hou, Y. Shi, and H.D. Sherali. Rate allocation and network lifetime problems for wireless sensor networks. *IEEE/ACM Trans. Netw.*, 16(2): 321–334, Apr. 2008.

[3] A. Kurs, A. Karalis, R. Moffatt, J.D. Joannopoulos, P. Fisher, and M. Soljacic. Wireless power transfer via strongly coupled magnetic resonances. *Science*, 317(5834): 83–86, July 2007.

[4] A. Kurs, R. Moffatt, and M. Soljacic. Simultaneous mid-range power transfer to multiple devices. *Appl. Phys. Lett.*, 96(4): article 044102, Jan. 2010.

[5] J. Luo and J.-P. Huabux. Joint mobility and routing for lifetime elongation in wireless sensor networks. In *Proc. IEEE INFOCOM*, pages 1735–1746, March 2005.

[6] R. C. Shah, S. Roy, S. Jain, and W. Brunette. Data MULEs: Modeling a three-tier architecture for sparse sensor networks. In *Proc. IEEE International Workshop on Sensor Network Protocols and Applications (SNPA)*, pages 30–41, May 2003.

[7] Y. Shi, and Y.T. Hou. Theoretical results on base station movement problem for sensor network. In *Proc. IEEE INFOCOM*, pages 376–384, Apr. 2008.

[8] Y. Shi, L. Xie, Y.T. Hou, and H.D. Sherali. On renewable sensor networks with wireless energy transfer. In *Proc. IEEE INFOCOM*, pages 1350–1358, Apr. 2011.

[9] E. Welzl. Smallest enclosing disks. *Lecture Notes in Computer Science (LNCS)*, 555: 359–370, 1991.

[10] L. Xie, Y. Shi, Y.T. Hou, W. Lou, H.D. Sherali, and S.F. Midkiff. On renewable sensor networks with wireless energy transfer: The multi-node case. In *Proc. IEEE SECON*, pages 10–18, June 2012.

[11] L. Xie, Y. Shi, Y.T. Hou, W. Lou, H.D. Sherali, and S.F. Midkiff. Bundling mobile base station and wireless energy transfer: Modeling and optimization. In *Proc. IEEE INFOCOM,* pages 1684–1692, Apr. 2013.

[12] L. Xie, Y. Shi, Y.T. Hou, W. Lou, and H.D. Sherali. On traveling path and related problems for a mobile station in a rechargeable sensor network. Technical Report, Department of Electrical and Computer Engineering, Virginia Tech, Blacksburg, VA, June 2013. Available at http://filebox.vt.edu/users/windgoon/papers/TR13.pdf.

[13] G. Xing, T. Wang, W. Jia, and M. Li. Rendezvous design algorithms for wireless sensor networks with a mobile base station. In *Proc. ACM MobiHoc,* pages 231–240, May 2008.

[14] W. Zhao, M. Ammar, and E. Zegura. A message ferrying approach for data delivery in sparse mobile ad hoc networks. In *Proc. ACM MobiHoc*, pages 187–198, May 2004.

APPENDIX

A. REFORMULATION

We show how to reformulate problem OPT-$\mathcal{L}$ to an LP via a change-of-variable technique. For the fractional objective function $\frac{\tau_{\text{vac}}}{\tau}$, we define $\eta_{\text{vac}} = \frac{\tau_{\text{vac}}}{\tau}$. We also define $\eta(\mathcal{L}_k) = \frac{\omega(\mathcal{L}_k)}{\tau}$ and $q = \frac{1}{\tau}$. For time constraint (8), we divide both sides by τ, and rewrite it as $\eta_{\text{vac}} + \sum_{k=1}^{K} \eta(\mathcal{L}_k) = 1$.

For (3) and (5), we consider logical points $\mathcal{L}_k, k = 1, 2, \cdots, K$, and p_{vac} separately. First, for $\mathcal{L}_k$, we multiple both sides of (3) by $\eta(\mathcal{L}_k)$ and define $g_{ij}(\mathcal{L}_k) = f_{ij}(\mathcal{L}_k) \cdot \eta(\mathcal{L}_k)$ and $g_{iB}(\mathcal{L}_k) = f_{iB}(\mathcal{L}_k) \cdot \eta(\mathcal{L}_k)$. For the new nonlinear terms $r_i(\mathcal{L}_k) \cdot \eta(\mathcal{L}_k)$, we define $\mathcal{E}_i(\mathcal{L}_k) = r_i(\mathcal{L}_k) \cdot \eta(\mathcal{L}_k)$. By the new variables $g_{ij}(\mathcal{L}_k)$, $g_{iB}(\mathcal{L}_k)$, and $\mathcal{E}_i(\mathcal{L}_k)$, (3) is reformulated as

$$\sum_{k \in \mathcal{N}}^{k \neq i} g_{ki}(\mathcal{L}_k) + R_i \cdot \eta(\mathcal{L}_k) = \sum_{j \in \mathcal{N}}^{j \neq i} g_{ij}(\mathcal{L}_k) + g_{iB}(\mathcal{L}_k) ,$$

and (5) is rewritten as

$$\mathcal{E}_i(\mathcal{L}_k) = \rho \sum_{k \in \mathcal{N}}^{k \neq i} g_{ki}(\mathcal{L}_k) + \sum_{j \in \mathcal{N}}^{j \neq i} C_{ij} \cdot g_{ij}(\mathcal{L}_k) \\ + C_{iB}(\mathcal{L}_k) \cdot g_{iB}(\mathcal{L}_k) .$$

Second, for p_{vac}, we multiply both sides of (3) and (5) by η_{vac}, and define $g_{ij}(p_{\text{vac}}) = f_{ij}(p_{\text{vac}}) \cdot \eta_{\text{vac}}, g_{iB}(p_{\text{vac}}) = f_{iB}(p_{\text{vac}}) \cdot \eta_{\text{vac}}$, and $\mathcal{E}_i(p_{\text{vac}}) = r_i(p_{\text{vac}}) \cdot \eta_{\text{vac}}$. Then (3) and (5) can be reformulated as

$$\sum_{k \in \mathcal{N}}^{k \neq i} g_{ki}(p_{\text{vac}}) + R_i \cdot \eta_{\text{vac}} = \sum_{j \in \mathcal{N}}^{j \neq i} g_{ij}(p_{\text{vac}}) + g_{iB}(p_{\text{vac}})$$

$$\mathcal{E}_i(p_{\text{vac}}) = \rho \sum_{k \in \mathcal{N}}^{k \neq i} g_{ki}(p_{\text{vac}}) + \sum_{j \in \mathcal{N}}^{j \neq i} C_{ij} \cdot g_{ij}(p_{\text{vac}}) \\ + C_{iB}(p_{\text{vac}}) \cdot g_{iB}(p_{\text{vac}})$$

By dividing both sides by τ, constraint (9) can be rewritten as $r_i(p_{\text{vac}}) \cdot \eta_{\text{vac}} + \sum_{k=1}^{K} r_i(\mathcal{L}_k) \cdot \eta(\mathcal{L}_k) \leq \sum_{k=1,\ldots,K}^{D_{iB}(p) \leq D_\delta, p \in \mathcal{A}_k^{u+c}} U_{iB}(\mathcal{L}_k) \cdot \eta(\mathcal{L}_k)$, or equivalently,

$$\mathcal{E}_i(p_{\text{vac}}) + \sum_{m=1}^{K} \mathcal{E}_i(\mathcal{L}_k) \leq \sum_{k=1,\ldots,K}^{D_{iB}(p) \leq D_\delta, p \in \mathcal{A}_k^{u+c}} U_{iB}(\mathcal{L}_k) \cdot \eta(\mathcal{L}_k)$$

Similarly, by dividing both sides by τ, (10) can be rewritten as $r_i(p_{\text{vac}}) \cdot \eta_{\text{vac}} + \sum_{k=1,\ldots,K}^{D_{iB}(p) > D_\delta, p \in \mathcal{A}_k^{u+c}} r_i(\mathcal{L}_k) \cdot \eta(\mathcal{L}_k) \leq \frac{E_{\max} - E_{\min}}{\tau}$, or equivalently,

$$\mathcal{E}_i(p_{\text{vac}}) + \sum_{k=1,\ldots,K}^{D_{iB}(p) > D_\delta, p \in \mathcal{A}_k^{u+c}} \mathcal{E}_i(\mathcal{L}_k) \leq (E_{\max} - E_{\min}) \cdot q .$$

Now the new objective function and new constraints are linear, which makes an LP.

B. PROOF OF LEMMA 3

PROOF. To show that $\psi_{\text{OPT-ub}} = (\tau, \tau_{\text{vac}}, \omega(p), f_{ij}(p), f_{iB}(p), r_i(p))$ is feasible to problem OPT-ub, we need to verify that $\psi_{\text{OPT-ub}}$ satisfies constraints $(3), (5), (8), (9),$ and (10). To do this, we exploit the worst case bounds that are inherited in a logical point representation.

Since $\psi_{\text{OPT-}\mathcal{L}}$ is feasible to problem OPT-$\mathcal{L}$ (based on the K logical points), we know that $\psi_{\text{OPT-}\mathcal{L}}$ satisfies constraints $(3), (5), (8), (9),$ and (10). We now verify each of these constraints for $\psi_{\text{OPT-ub}}$. Since τ and τ_{vac} remain unchanged and $\omega(p_k) = \omega(\mathcal{L}_k)$, where $p_k \in \mathcal{A}_k^{u+c}, 1 \leq k \leq K$, $\psi_{\text{OPT-ub}}$ satisfies constraint (8). $\psi_{\text{OPT-ub}}$ also satisfies constraints (3) and (5) since $f_{ij}(p_{\text{vac}})$, $f_{iB}(p_{\text{vac}})$ and $r_i(p_{\text{vac}})$ remain unchanged, $f_{ij}(p_k) = f_{ij}(\mathcal{L}_k)$, $f_{iB}(p_k) = f_{iB}(\mathcal{L}_k)$, and $r_i(p_k)$ is determined by (5).

To verify two remaining energy constraints (9) and (10), by (19) and (22), we first have $C_{iB}(p_k) \leq C_{iB}(\mathcal{L}_k), 1 \leq k \leq K$. As a result, $r_i(p_k) = \rho \sum_{k \in \mathcal{N}}^{k \neq i} f_{ki}(p_k) + \sum_{j \in \mathcal{N}}^{j \neq i} C_{ij} \cdot f_{ij}(p_k) + C_{iB}(p_k) \cdot f_{iB}(p_k) \leq \rho \sum_{n \in \mathcal{N}}^{n \neq i} f_{ni}(\mathcal{L}_k) + \sum_{j \in \mathcal{N}}^{j \neq i} C_{ij} \cdot f_{ij}(\mathcal{L}_k) + C_{iB}(\mathcal{L}_k) \cdot f_{iB}(\mathcal{L}_k) = r_i(\mathcal{L}_k)$, where the first equality holds since $\psi_{\text{OPT-ub}}$ satisfies (5), the second equality holds since $f_{ij}(p_k) = f_{ij}(\mathcal{L}_k)$, $f_{iB}(p_k) = f_{iB}(\mathcal{L}_k)$ and $C_{iB}(p_k) \leq C_{iB}(\mathcal{L}_k)$, and the last equality holds since $\psi_{\text{OPT-}\mathcal{L}}$ satisfies (5). By the same token, we have that $r_i(p_{\text{vac}})$ is unchanged since $C_{iB}(p_{\text{vac}})$ is unchanged.

Since $r_i(p_k) \leq r_i(\mathcal{L}_k)$ and $r_i(p_{\text{vac}})$ is unchanged, we have

$$\begin{aligned} &r_i(p_{\text{vac}}) \cdot \tau_{\text{vac}} + \sum_{k=1}^{K} r_i(p_k) \cdot \tau(p_k) \\ \leq \quad &r_i(p_{\text{vac}}) \cdot \tau_{\text{vac}} + \sum_{k=1}^{K} r_i(\mathcal{L}_k) \cdot \tau(\mathcal{L}_k) \\ \leq \quad &\sum_{k=1,\ldots,K}^{D_{iB}(p) \leq D_\delta, p \in \mathcal{A}_k^{u+c}} U_{iB}(\mathcal{L}_k) \cdot \tau(\mathcal{L}_k) \\ \leq \quad &\sum_{k=1,\ldots,K}^{D_{iB}(p_k) \leq D_\delta} U_{iB}(p_k) \cdot \tau(p_k) \end{aligned}$$

where the first inequality holds since $r_i(p_{\text{vac}})$ and τ_{vac} are unchanged, $r_i(p_k) \leq r_i(\mathcal{L}_k)$ and $\tau(p_k) = \tau(\mathcal{L}_k)$, the second inequality holds since $\psi_{\text{OPT-}\mathcal{L}}$ meets (9), the third inequality holds by $U_{iB}(\mathcal{L}_k) \leq U_{iB}(p_k)$ (see (15) and (21)) and $\tau(p_k) = \tau(\mathcal{L}_k)$. Thus, constraint (9) holds for $\psi_{\text{OPT-ub}}$. Similarly, we can show that constraint (10) holds for $\psi_{\text{OPT-ub}}$. Therefore, the constructed solution $\psi_{\text{OPT-ub}}$ is feasible to problem OPT-ub. This completes the proof. $\square$